




Article

An Experimental Study on Vortex-Induced Vibration Suppression of a Long Flexible Catenary Cable by Using Vibration Dampers

Li Ruan ^{1,*} , Hongzhong Zhu ²  and Changhong Hu ² 

¹ Interdisciplinary Graduate School of Engineering Sciences, Kyushu University, Kasuga, Fukuoka 816-8580, Japan

² Research Institute for Applied Mechanics, Kyushu University, Kasuga, Fukuoka 816-8580, Japan; zhuhongzhong@riam.kyushu-u.ac.jp (H.Z.); hu@riam.kyushu-u.ac.jp (C.H.)

* Correspondence: ruanli19910225@gmail.com

Abstract: In this paper, an experimental study is conducted to investigate the effectiveness of vibration dampers in suppressing vortex-induced vibration in a long, flexible catenary cable with a low mass ratio. The dampers, consisting of two small, symmetric, lightweight pipes clamped to the cable, are sparsely deployed along the cable to shape the vibration characteristics. The experimental results demonstrate that dampers significantly reduce the vibration amplitude by up to 60% and axial tension by up to 61% at high flow velocities, effectively suppressing the cable vibration in perpendicular flow. In addition, it is observed that the in-line and cross-flow vibration frequencies are approximately equal when the dampers are applied. This behavior contrasts with the conventional undamped catenary cable, where the in-line vibration frequencies are double those of the cross-flow frequencies.

Keywords: vortex-induced vibration (VIV); vibration damper; VIV suppression; axially varying tension; flexible catenary cable



Citation: Ruan, L.; Zhu, H.; Hu, C. An Experimental Study on Vortex-Induced Vibration Suppression of a Long Flexible Catenary Cable by Using Vibration Dampers. *J. Mar. Sci. Eng.* **2024**, *12*, 1995. <https://doi.org/10.3390/jmse12111995>

Academic Editors: Xiangshao Kong and Weiguo Wu

Received: 24 September 2024

Revised: 1 November 2024

Accepted: 3 November 2024

Published: 6 November 2024



Copyright: © 2024 by the authors. Licensee MDPI, Basel, Switzerland. This article is an open access article distributed under the terms and conditions of the Creative Commons Attribution (CC BY) license (<https://creativecommons.org/licenses/by/4.0/>).

1. Introduction

Vortex-induced vibration (VIV) is a common fluid–structure coupling problem affecting high-aspect-ratio subsea structures, such as mooring lines, deep-sea risers, subsea pipelines, and submarine cables. When subjected to ocean currents, these structures can experience vortex shedding, which alters the surrounding flow field and generates oscillatory hydrodynamic forces. If the vortex shedding frequency approaches the structure’s natural frequency, a lock-in phenomenon may occur, significantly amplifying these forces [1,2]. This can reduce the fatigue life or, in extreme cases, cause structural failure [3,4]. Therefore, understanding VIV responses and developing effective suppression techniques is critical for the safety of slender subsea structures.

VIV suppression for high-aspect-ratio subsea structures can be achieved by active or passive methods. Active methods typically use a control system to introduce external forces that disrupt vortex shedding, such as cylinder rotational oscillations, suction and injection, and acoustic excitation [5,6]. In contrast, passive suppression techniques, including helical strakes, buoyancy modules, and splitter plates, rely on adding components to structures, to mitigate vortex shedding or axial tension [7–11]. As the passive techniques do not require additional power and ease of manufacturing and implementation, they are widely adopted in practical applications [12–15].

To analyze the effectiveness of VIV suppression techniques, common approaches include experimental observation [16,17], semi-empirical theoretical models [18], and computational fluid dynamics (CFD) simulations [19]. Semi-empirical models often derive empirical parameters from forced vibration tests using rigid smooth cylinders. However, differences between experimental conditions and practical situations make the semi-empirical

model less suitable for studying the VIV phenomena of flexible cables with suppression devices [19]. In CFD approaches, the interaction between bare cylinder structures and their suppression devices is not explicitly considered, resulting in noticeable discrepancies between simulation and experimental results [20,21]. Hence, approaches based on experimental observation remain the preferred methods for studying VIV suppression. Ma et al. reported that varying axial excitation for a flexible horizontal cylinder could weaken the VIV suppression efficiency of helical strakes [22]. Guo et al. experimentally investigated the VIV suppression effectiveness of a sleeve suppression device for a flexible inclined cylinder and found that the sleeve coverage could affect the VIV suppression effectiveness [23]. Xu et al. explored the optimal deployment of helical strakes for a flexible inclined riser and found that the VIV suppression effectiveness of the helical strakes gradually decreases as the angle between the plane orthogonal to the incoming flow and the cylinder axis increases [24,25].

This study experimentally investigates a passive vibration suppression method for a flexible cable using vibration dampers. The damper design features two small, symmetric, lightweight hollow ends connected by a rigid strand, which increases local added mass and damping. The dampers are sparsely deployed along the cable to shape the cable vibration characteristics. As the dampers extend outward from the cable and would be vulnerable to impact, they are not intended for installation in extremely harsh conditions. In the experiment, various flow velocities are considered in the experiments while the cable vibration amplitudes, frequencies, and axial tension are explored. The variation in axial tension of the cable is an important target of this research, which has not been well studied so far experimentally, although there has been some research on the mooring lines by numerical methods [26,27]. In addition, although vibration suppression by additional dampers, such as the Stockbridge dampers [28,29], has been widely investigated and implemented on overhead power lines [30–35] to reduce the effect of the galloping phenomenon, its applications to marine cables remain unexplored, to the best of the authors' knowledge.

The remainder of this paper is organized as follows. The experimental system is described in Section 2. In Section 3, the experimental results and discussion are presented. Finally, this study is summarized in Section 4.

2. Experimental System

The marine cable studied in [36–38] is accounted for in this study. The main parameters are given in Table 1. A 1/10 experimental model is developed for this study, as shown in Figure 1. The prototype cable is a typical three-phase AC submarine power cable. The model is made based on the hydro-elastic similarity law. The geometric similarity ratio is taken as 1:10. To ensure the similarity between the prototype and model, the density similarity ratio is 1:1 and the similarity ratio of the elastic modulus is equal to the similarity ratio of the geometry. In the experimental model, a carbon rod with a diameter of 1.5 mm is used as the central axis of the cable model to imitate the bending and axial stiffness. Aluminum lumps and plastic lumps with a diameter of 20 mm and a length of 10 mm are installed along the carbon rod. In the center of each aluminum lump and plastic lump, a hole with a diameter of 1.5 mm is machined for the assembly. Small washers are placed between the lumps to prevent the lumps from bumping in cable bending. In order to make the surface of cable model smooth, the cable model is covered by a plastic membrane. Additionally, twelve red markers, spaced 10 cm apart, are placed on the cable model for cable motion tracking. To measure the axial tension, two load cells are assembled at the ends of the cable, as shown in Figure 1a. The cable model's total length is 1.38 m, the horizontal distance between cable ends is 1.3 m, and the vertical height between cable ends is 0.4 m. The diagram of the experimental model is shown in Figure 2, and the set-up of the experimental model is shown in Figure 3.

Table 1. Main properties of cable model.

Parameter	Value		Unit
	Prototype	Model	
Cable diameter, D	0.2	0.02	m
Cable mass per unit length	72	0.65	kg/m
Mass ratio *	2.236	2.0253	—
Bending stiffness, EI	10,000	0.08	Nm ²
Axial stiffness, EA	700×10^6	500,000	N
Minimum Bend Radius	2	2.176	m
Damping ratio, ξ		0.08	—
Natural frequency, f_n		3.1	Hz
top tension		8.34	N
top angle		32.4	°

* Mass ratio is the ratio of the cable to the mass of the displaced water.

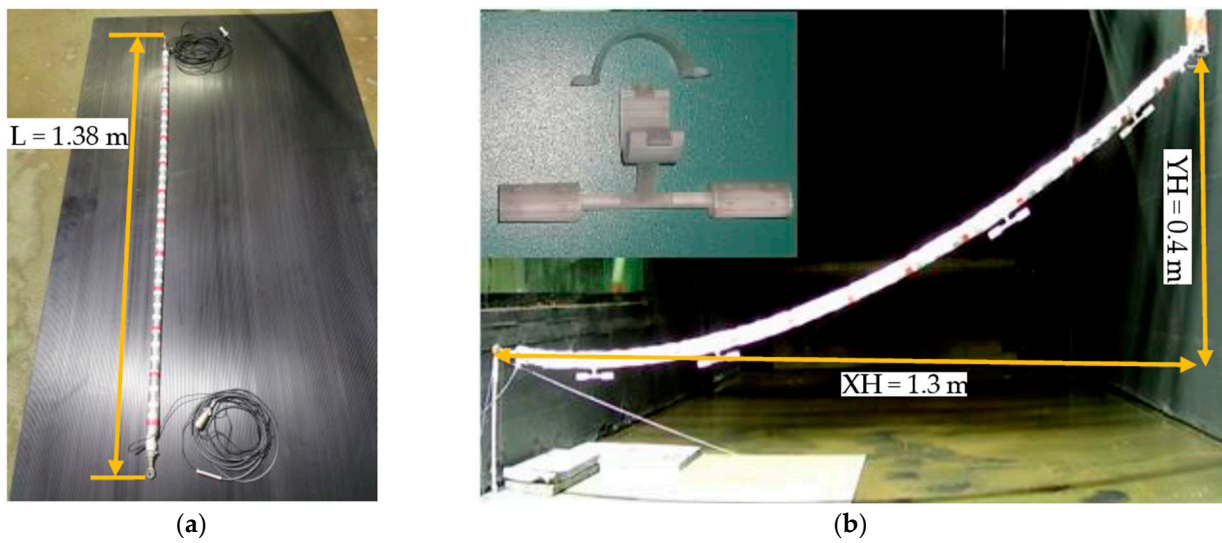


Figure 1. Cable model: (a) experimental model; (b) cable model with the vibration dampers.

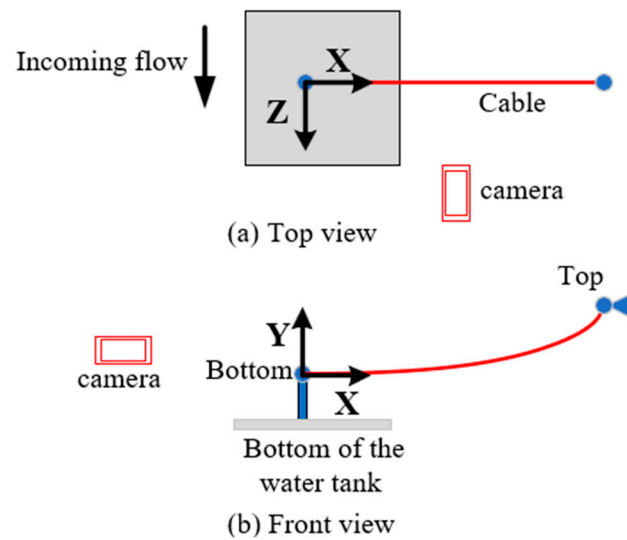


Figure 2. Experimental set-up overview: (a) top view; (b) front view.



Figure 3. Experimental overall framework in (left) and outside (right) the water tank.

In this study, cable response in perpendicular flow is studied. The coordinate frame is defined at the lower end of the cable model, with its Y-axis pointing upwards and Z-axis aligning with the incoming flow direction, as shown in Figure 2. The X-axis is determined by the right-hand rule. Initially in calm water, the cable sags in the X–Y plane, and its profile forms a classical hyperbolic curve. The top end of the cable model is hinged to an external fixed structure and the bottom end is hinged to an aluminum rod fixed at the base of the water tank. Two video cameras (model: WTW-WA320H) are employed to capture the in-line and cross-flow motion of the cable, as shown in Figure 3.

The vibration damper proposed for this study is depicted in Figure 1b. It consists of two small elliptical cylinders at the two ends and a rigid strand in the middle. A clamp, composed of two semicircular laminates that can be assembled by bolts, is applied to tie the damper to the cable. The elliptical cylinders are designed to be hollow but filled with surrounding water to increase the oscillating mass. The damper is made of resin by a 3D printer. The length of the major and minor axes of the elliptical cylinder is 10 mm and 5 mm, respectively, and each elliptical cylinder is 20 mm length. The strand’s length and diameter are 30 mm and 3.5 mm. The damper mass and its wet mass are 4 g and 0.5 g, respectively. This lightweight design of the damper can help the cable keep its catenary profile in calm water while improving the added mass and damping during vibration. As shown in Figure 4, four dampers are symmetrically installed on the cable, located at 0.22 m, 0.44 m, 0.95 m, and 1.19 m.

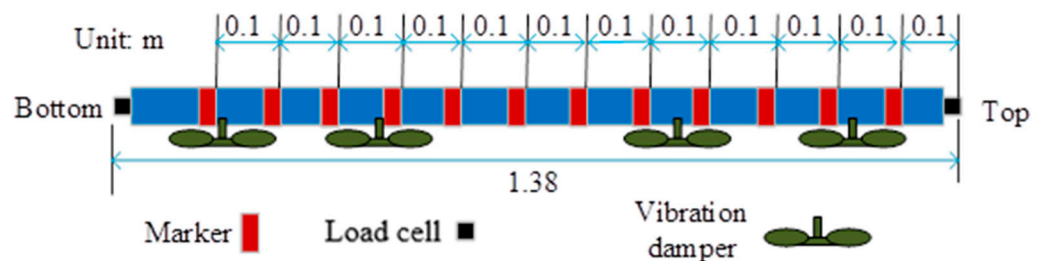


Figure 4. Diagram of the cable model with the vibration dampers.

The experiments are performed in the circulating water tank at the Research Institute for Applied Mechanics (RIAM) of Kyushu University. The water tank features a 5 m long, 1.5 m wide, and 2 m deep test section. A free-decay test is initially carried out in still water to measure the cable model’s natural frequency [39]. In experiments, the cables with and without vibration dampers are studied. The incoming flow velocities range from 0.2 m/s to 0.6 m/s, increasing in 0.04 m/s increments, corresponding to a Reynolds number between

4000 and 12,000 based on the cable model diameter. Each test is carried out twice to increase the reliability of the measurements. The cable motion is captured and analyzed using an open-source video processing software Tracker [40].

3. Results

In this section, the experimental results for the cable with and without vibration dampers are analyzed. Since the vibration damper has a very light wet weight (approximately 0.5 g), the initial static profile and local inclination angle of the cable with vibration dampers remain nearly identical to those of the cable without vibration dampers. In data processing, the averaged offset of the cable from its initial position is removed to ensure consistency in the comparison. For ease of explanation, the displacements in the X, Y, and Z directions are denoted by u , v , and w .

3.1. Response of Vibration

The maximum displacements under various flow velocities are compared, as shown in Figure 5. It is noteworthy that the vibration frequencies in the Z-axis exceed the Nyquist sampling frequency, the vibration amplitude of the cable under $U_0 = 0.60$ m/s is not plotted in Figure 5a.

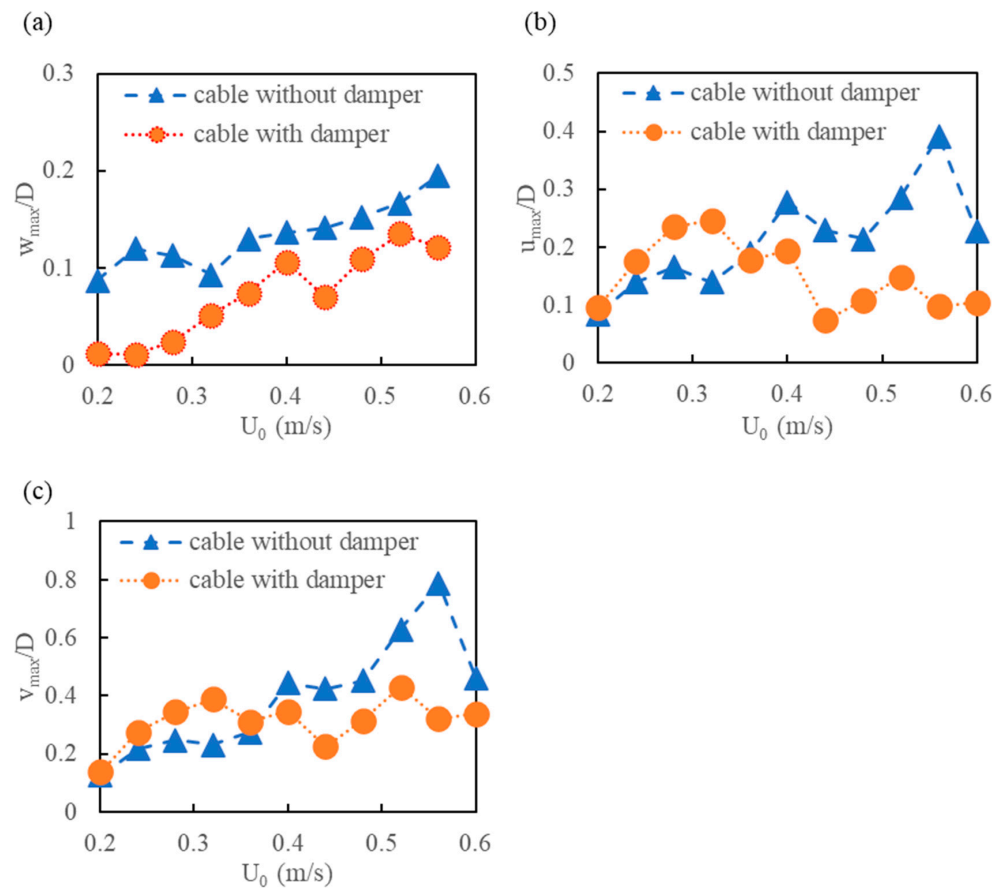


Figure 5. Maximum displacements from the experimental results for cables without and with vibration dampers under various flow velocities: (a) in-line displacements w_{max} ; (b) cross-flow displacements u_{max} ; (c) cross-flow displacements v_{max} .

The maximum displacements show a different tendency between the cables with and without vibration dampers. As shown in Figure 5a, the maximum displacements of the cable with vibration dampers are always smaller under all the flow velocities in the in-line w direction, and the maximum displacements can be reduced by 87% under $U_0 = 0.2$ m/s. In cross-flow directions under 0.36 m/s $< U_0 \leq 0.6$ m/s, as shown in Figure 5b,c, the

maximum displacements can be significantly reduced, though the values are slightly enlarged under $U_0 \leq 0.36$ m/s. In the cross-flow direction under $U_0 = 0.56$ m/s, the maximum displacements decrease by 75% and 60% in the X- and Y-directions, respectively.

It is worth noting that the maximum displacements of the cable with vibration dampers rapidly decrease in all cases under $U_0 = 0.44$ m/s, as depicted in Figure 5. In addition, the maximum responses in the Y-direction consistently exhibit the largest displacements under all flow velocities. For the cable without dampers, the maximum displacements in the lock-in region under 0.36 m/s $\leq U_0 < 0.6$ m/s are greater than those outside the region. In contrast, the maximum displacements for the cable with dampers are smaller than those outside this region.

The maximum root-mean-squared (RMS) displacements are compared in Figure 6. The maximum RMS displacements vary similarly with the maximum displacements. The responses in the Y-direction consistently exhibit the largest displacements under all flow velocities. In the cross-flow direction under $U_0 = 0.56$ m/s, the maximum RMS displacements is reduced by 64.4% and 46.4%, respectively, in the X- and Y-directions. The vibration amplitudes decrease by 68% in the in-line w direction under $U_0 = 0.2$ m/s.

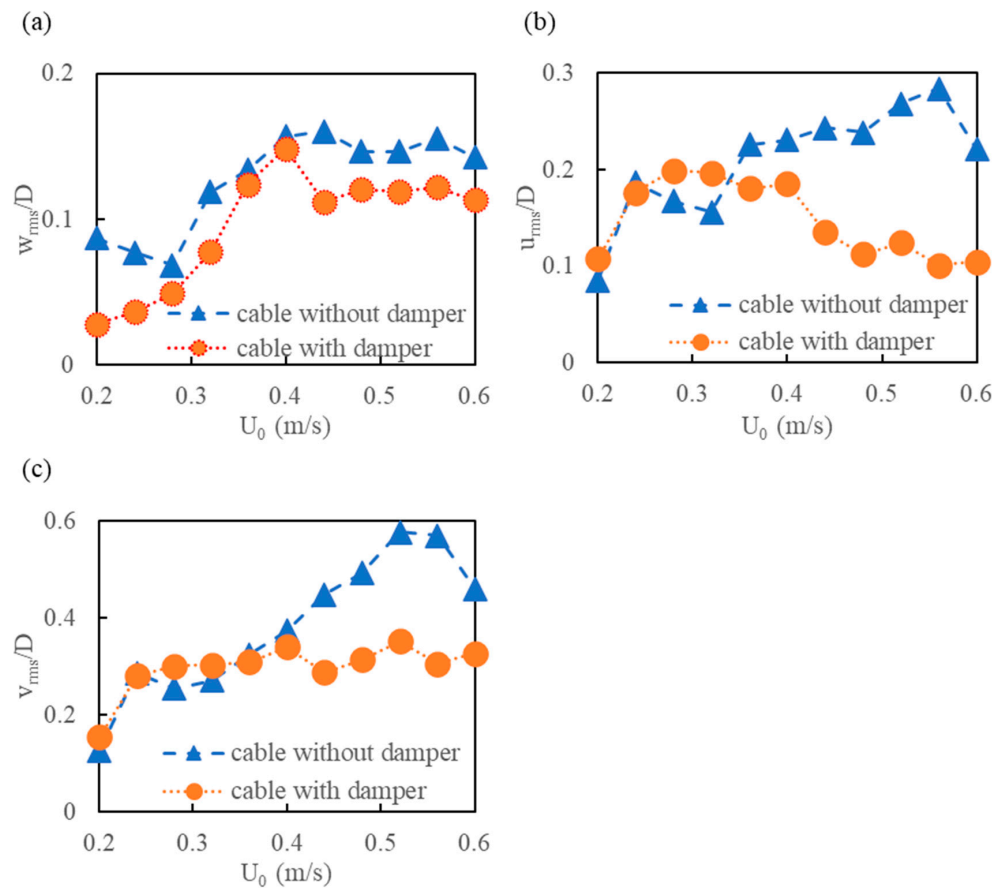


Figure 6. Maximum RMS displacements from the experimental results for the cable with and without vibration dampers: (a) in-line RMS displacements w_{rms} ; (b) cross-flow RMS displacements u_{rms} ; (c) cross-flow RMS displacements v_{rms} .

The time-averaged in-line displacements of the experimental results are shown in Figure 7. As the flow velocity increases, the time-averaged equilibrium profiles progressively deviate from the initial position (Y-axis). It is worth noting that at low flow velocities $U_0 \leq 0.24$ m/s, the time-averaged in-line displacements of the cable with dampers are larger. As U_0 increases, the results are reversed. It is worth noting that the time-averaged equilibrium profiles are almost constant under $U_0 \geq 0.56$ m/s for the cable without vibration dampers, and the in-line displacements reach their maximum value.

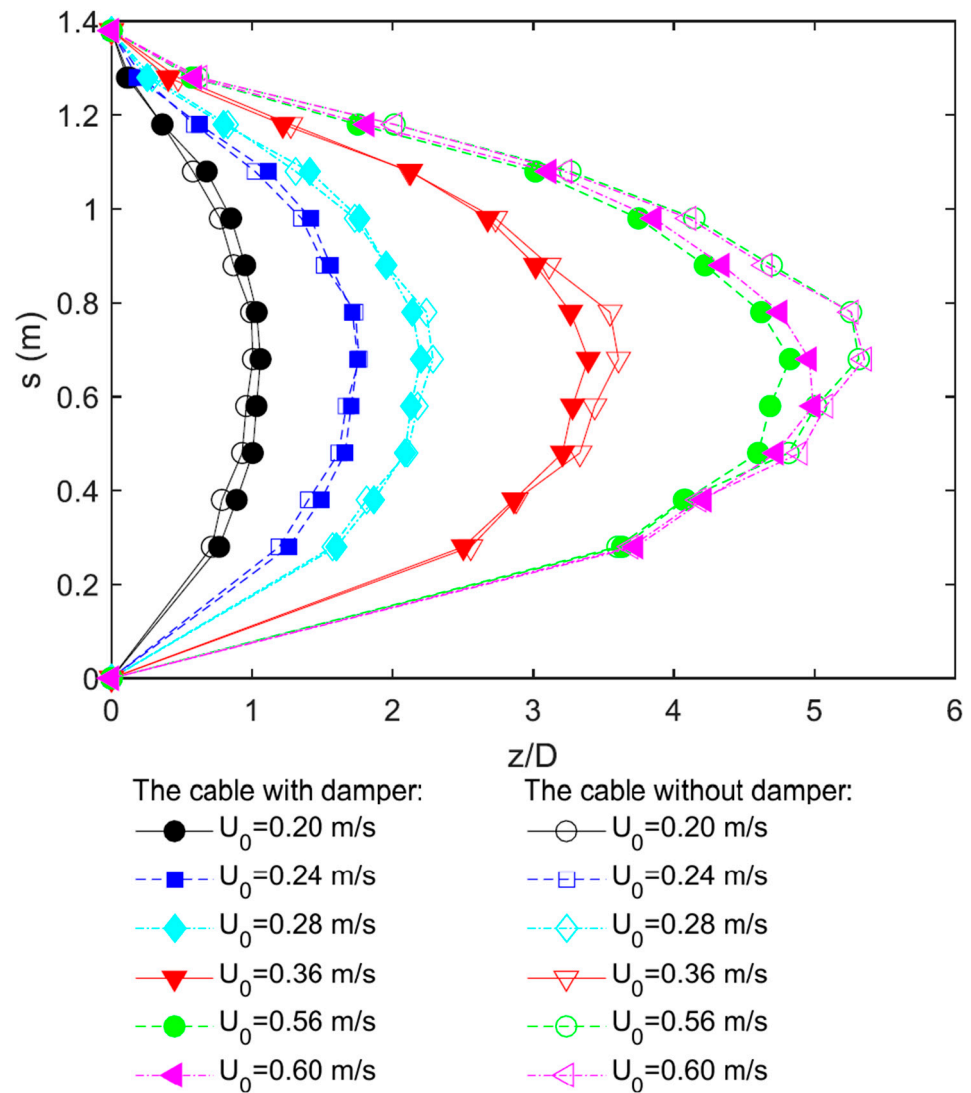


Figure 7. Comparison of the time-averaged in-line displacements from experimental results for the cable with and without vibration dampers (solid marks represent the cables with vibration dampers and hollow marks represent the cables without vibration dampers).

The cable’s oscillating frequencies are compared in Figures 8 and 9. As shown in Figure 8, the oscillating frequencies in the X- and Y-directions are consistently equal under all flow velocities. The ratio of cross-flow oscillation frequency to the natural frequency (f_n) approaches 1 under $U_0 = 0.36$ m/s, indicating that the cable enters the lock-in region. At low flow velocities $U_0 \leq 0.40$ m/s, the cross-flow oscillation frequencies of the cables with and without vibration dampers are almost equal. As U_0 increases, the cross-flow oscillation frequencies of the cable with vibration dampers increase rapidly and become greater than those of the cable without dampers.

As shown in Figure 9, the in-line oscillation frequencies are roughly double the cross-flow oscillation frequencies for the cable without vibration dampers. On the other hand, the in-line and cross-flow oscillation frequencies are nearly the same for the cable with vibration dampers. Therefore, it is observed that the vibration dampers significantly influence the resonance frequency ratio between the in-line and cross-flow oscillations.

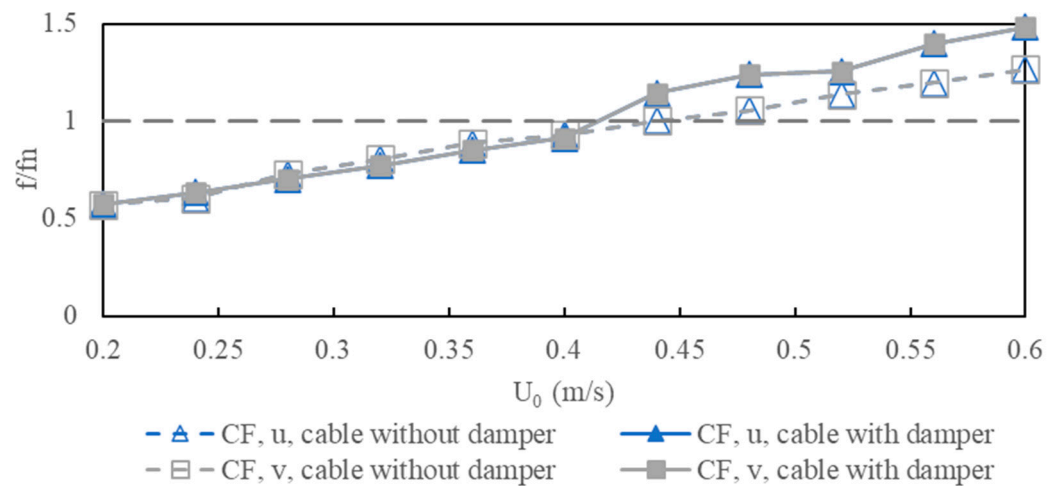


Figure 8. Comparison of the frequency ratio in the cross-flow direction for the cables with and without vibration dampers.

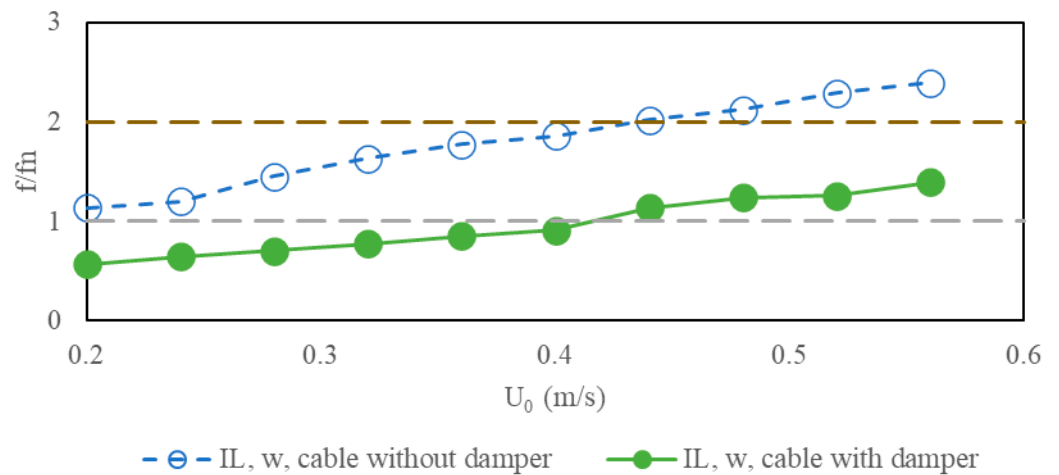


Figure 9. Comparison of the frequency ratio in the in-line w direction of experimental results for the cables with and without vibration dampers.

3.2. Response of Tensions

In the experiment, the tension at both ends of the cable under $U_0 = 0.56$ m/s and the associated results in the frequency domain are presented in Figures 10 and 11 for the cable without and with vibration dampers, respectively. In order to reduce the effects caused by sensor drift, the measurements are reset before each experiment. As shown in Figures 10 and 11, the tension at both ends of the cable oscillates in-phase, with nearly identical frequencies. Additionally, the tension at the upper end of the cable is slightly larger than that at the lower side. It is obvious that the time-history tensions in the cable without vibration dampers are much larger than those in the cable with vibration dampers. In the cable without vibration dampers, the second frequency of tension is the dominant frequency. In contrast, the first frequency of tension is the dominant frequency for the cable with vibration dampers. The tension oscillating frequencies of the cable with vibration dampers is slightly greater than those of the cable without dampers. These are consistent with the vibration frequencies in Figures 8 and 9. Therefore, the vibration dampers can reduce the tension amplitude and change the vibration characteristics.

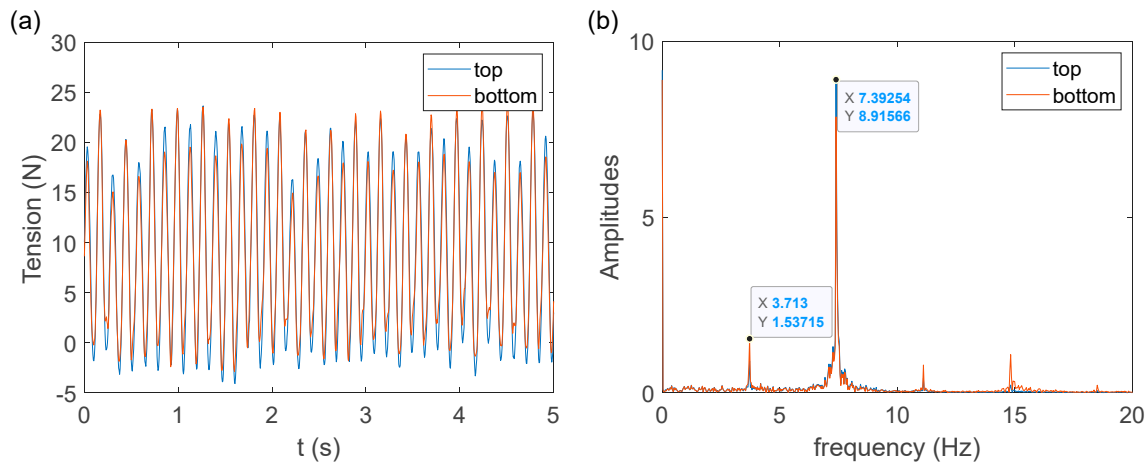


Figure 10. Tension at the ends of the cable without vibration dampers at $U_0 = 0.56$ m/s: (a) Time-history results and (b) Frequency-domain results.

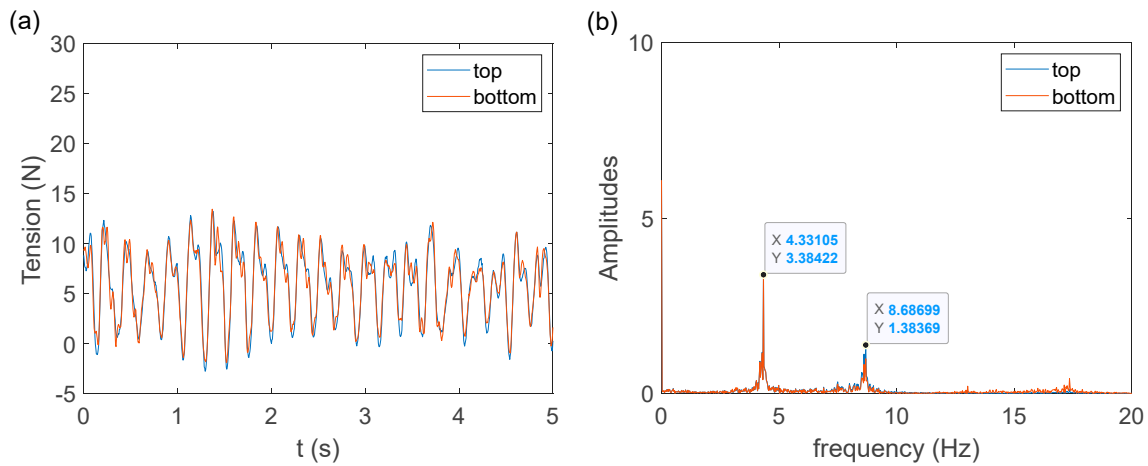


Figure 11. Tension at the ends of the cable with vibration dampers at $U_0 = 0.56$ m/s: (a) Time-history results and (b) Frequency-domain results.

The averaged tension with the flow velocity U_0 is compared in Figure 12. It can be seen that the averaged tension increases as the flow velocity U_0 increases. Meanwhile, the averaged tension at both ends of the cable with and without vibration dampers is nearly identical under all the flow velocities, except $U_0 = 0.52$ m/s. This would be caused by the measurement error. Like the vibration displacement response in Figures 5 and 6, at low flow velocity ($U_0 \leq 0.36$ m/s), the time-averaged tension of the cable with vibration dampers is larger. And at high flow velocity ($U_0 > 0.36$ m/s), the time-averaged tension of the cable without dampers increases rapidly and becomes larger than that of the cable with dampers. Under $U_0 = 0.56$ m/s, the averaged tension of the cable with vibration dampers decreases by 34% compared to the case without dampers.

The maximum amplitudes of the tension variation with the flow velocity U_0 are compared in Figure 13. The results show that the maximum amplitudes of the tension variation of the cable without vibration dampers are much larger than those of the cable with vibration dampers as the flow velocity increases. For the cable with vibration dampers, the maximum amplitudes of the tension variation show slight variations as the flow velocity U_0 increases under $U_0 \geq 0.40$ m/s. In addition, the tension amplitudes at the upper end of the cable decreases by 61.5% under $U_0 = 0.56$ m/s.

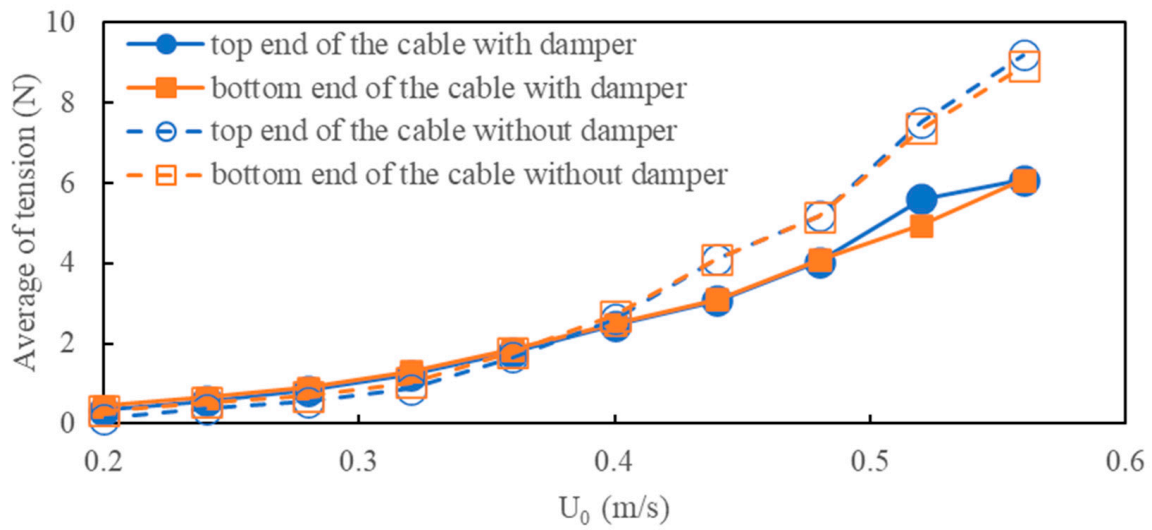


Figure 12. Average of tension at both ends of the cable without vibration dampers and the cable with vibration dampers.

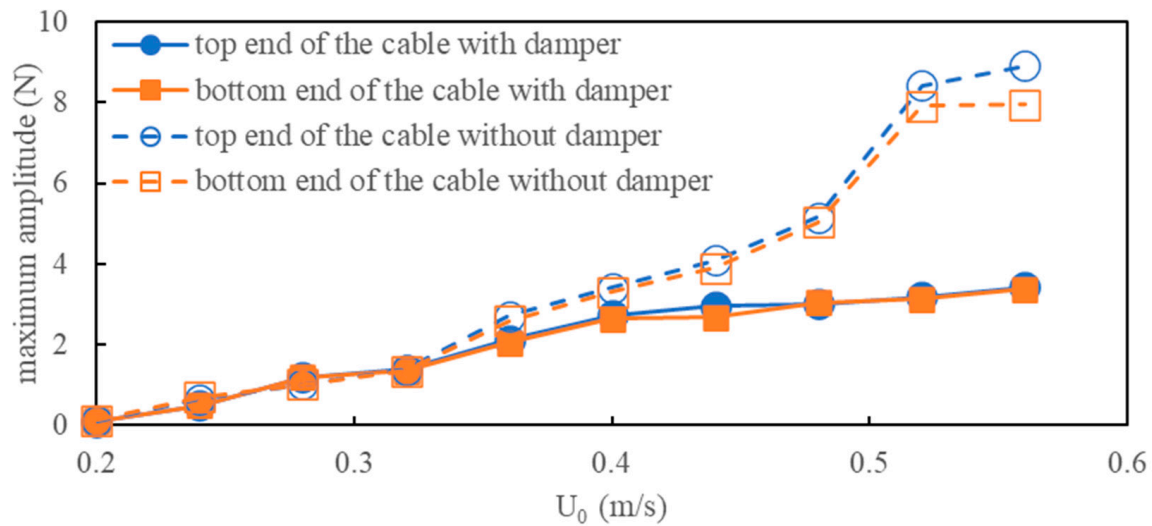


Figure 13. Maximum amplitudes of the tension variation at both ends of the cable without vibration dampers and the cable with vibration dampers.

The tension frequencies at the ends of the cable are compared in Figure 14. The results indicate that the tension frequencies at the top and bottom ends of the cable are almost the same at all flow velocities for both ends of the cable with and without vibration dampers. As the flow velocity increases, the tension frequency increases. Additionally, compared to Figure 9, it can be seen that the tension frequencies are approximately the same as the in-line oscillation frequencies.

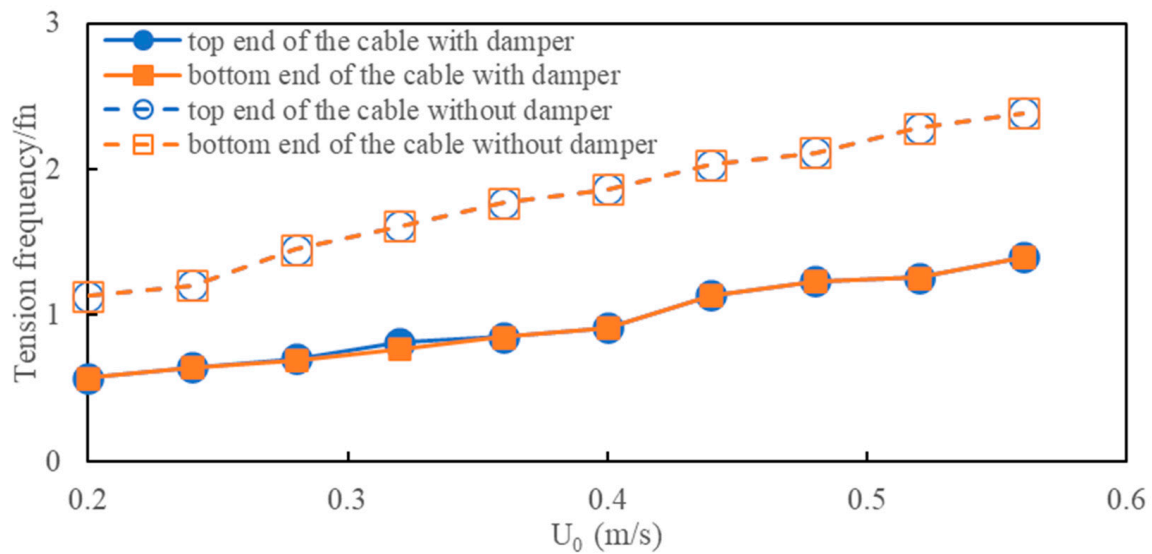


Figure 14. Tension frequencies at both ends of the cable without vibration damper and the cable with vibration damper.

4. Conclusions

In this study, an experiment on a submarine cable model was conducted to study VIV suppression by vibration dampers. The experimental results of the cable with and without vibration dampers in perpendicular flow are compared for the VIV responses on maximum displacement, axial tension, and corresponding frequencies. The experimental results indicate that both the maximum displacement and the cable axial tension can be remarkably reduced under high flow velocities, though the values are slightly enlarged under low flow velocities. Additionally, the vibration dampers significantly change the vibration frequency of the cable.

The key conclusions derived from this study are as follows:

For the experiments with and without vibration dampers, the maximum displacements and maximum RMS displacements show similar tendencies in three (X, Y, and Z) directions as the flow velocity U_0 increases. Due to the vibration dampers, the maximum displacements in the three (X, Y, and Z) directions can be reduced by up to 75%, 60%, and 87%, respectively. The maximum RMS displacements in the three (X, Y, and Z) directions can be reduced by up to 64.4%, 46.4%, and 68%, respectively. Under all the flow velocities, the cross-flow oscillation frequencies in the X direction remain identical to those in the Y direction. For the cable with vibration dampers, the in-line and cross-flow oscillation frequencies are approximately the same, while for the cable without vibration dampers, the in-line oscillation frequencies are about double those of the cross-flow oscillation frequencies.

For the experiments with and without vibration dampers, the tension at both ends of the cable oscillates in-phase, with nearly identical frequencies. The average, maximum amplitude, and frequency of tension increase as the flow velocity increases. The frequencies of tension are the same as the in-line cable oscillation frequencies. The tension time history of the cable without vibration dampers is much larger than that of the cable with vibration dampers. With the cable with vibration dampers, the average of tension can be reduced by up to 34%, and the tension maximum amplitude decreases by 61.5%.

In this preliminary study, the effectiveness of the dampers has been confirmed. It is anticipated that the geometry of the dampers and their layout along the cable could significantly influence VIV suppression performance. Optimizing the damper design and layout will be a focus of future work.

Author Contributions: Conceptualization, H.Z. and C.H.; data curation, L.R.; formal analysis, L.R.; funding acquisition, C.H.; investigation, L.R. and H.Z.; methodology, L.R. and H.Z.; resources, C.H.; supervision, C.H.; validation, H.Z. and C.H.; writing—original draft preparation, L.R.; writing—review and editing, H.Z. and C.H. All authors have read and agreed to the published version of the manuscript.

Funding: This research received no external funding.

Institutional Review Board Statement: Not applicable.

Informed Consent Statement: Not applicable.

Data Availability Statement: Data will be made available on request.

Conflicts of Interest: The authors declare no conflicts of interest.

References

- Li, R.; Karma, M.; Hu, C. Two-Dimensional VIV Simulation of a Cylinder Close to a Wall with High Reynolds Number by Overset Mesh. *Evergreen* **2023**, *10*, 219–229. [\[CrossRef\]](#)
- Gu, J.; Vitola, M.; Coelho, J.; Pinto, W.; Duan, M.; Levi, C. An experimental investigation by towing tank on VIV of a long flexible cylinder for deepwater riser application. *J. Mar. Sci. Technol.* **2013**, *18*, 358–369. [\[CrossRef\]](#)
- Ruan, L.; Zhu, H.; Hu, C. A study on vortex-induced vibration of a long flexible catenary cable in perpendicular flow. *Ocean. Eng.* **2024**, *305*, 117937. [\[CrossRef\]](#)
- Zhang, M.; Fu, S.; Song, L.; Tang, X.; He, Y. A time domain prediction method for the vortex-induced vibrations of a flexible riser. *Mar. Struct.* **2018**, *59*, 458–481. [\[CrossRef\]](#)
- Gao, Y.; Fu, S.; Song, L.; Peng, T.; Lei, R. Experimental investigation on the suppression device of VIV of a flexible riser. In Proceedings of the ASME 2014 33rd International Conference on Ocean, Offshore and Arctic Engineering, San Francisco, CA, USA, 8–13 June 2014; Volume 45400. [\[CrossRef\]](#)
- Lou, M.; Chen, Z.; Chen, P. Experimental investigation of the suppression of vortex induced vibration of two interfering risers with splitter plates. *J. Nat. Gas Sci. Eng.* **2016**, *35*, 736–752. [\[CrossRef\]](#)
- Zheng, H.; Wang, J. A numerical study on the vortex-induced vibration of flexible cylinders covered with differently placed buoyancy modules. *J. Fluids Struct.* **2021**, *100*, 103174. [\[CrossRef\]](#)
- Yuan, Y.; Zhuang, C.; Tang, W.; Xue, H. Numerical investigation of Vortex-Induced Vibration response for a full-scale riser with staggered buoyancy modules. *Ocean. Eng.* **2022**, *252*, 111241. [\[CrossRef\]](#)
- Sun, Y.Y.; Chen, G.M.; Chang, Y.J. Riser buoyancy distribution optimization based on vortex-induced vibration suppression. *J. China Univ. Pet.* **2009**, *33*, 123–127. [\[CrossRef\]](#)
- Chang, Y. *Design Approach and Its Application for Deepwater Drilling Risers*; University of Petroleum: Dongying, China, 2008. [\[CrossRef\]](#)
- Zhou, Y.; Yi, Q.; Wang, L.P.; Wang, D.S.; Yin, Y.S.; Dong, L.H. Preparation and strength analysis of buoyancy materials for deep-sea drilling riser. *J. Chongqing Univ.* **2017**, *40*, 19–24. [\[CrossRef\]](#)
- Liu, Q.; Hao, W.; Li, C.; Miao, W.; Ding, Q. Numerical simulation on the forced oscillation of rigid riser with helical strakes in different section shapes. *Ocean. Eng.* **2019**, *190*, 106439. [\[CrossRef\]](#)
- Liu, X.; Wang, X.; Jiang, Y.; Chen, G.; Xu, L.; Li, C. An optimization method for the suppression device configuration of risers. *Ocean. Eng.* **2019**, *194*, 106619. [\[CrossRef\]](#)
- Song, J.; Chen, W.; Guo, S.; Yan, D. Study on suppressing the vortex-induced vibration of flexible riser in frequency domain. *Appl. Ocean. Res.* **2021**, *116*, 102882. [\[CrossRef\]](#)
- Jiang, Z.; Li, P.; Feng, L.; Wang, Y.; Liu, L.; Guo, H. Experimental investigation on the VIV of two side-by-side risers fitted with triple helical strakes under coupled interference effect. *J. Fluids Struct.* **2021**, *101*, 103202. [\[CrossRef\]](#)
- Fang, S.M.; Niedzwecki, J.M.; Fu, S.; Li, R.; Yang, J. VIV response of a flexible cylinder with varied coverage by buoyancy elements and helical strakes. *Mar. Struct.* **2014**, *39*, 70–89. [\[CrossRef\]](#)
- Li, A.; Wu, B.; Fan, D. Vortex-induced vibration of risers with staggered buoyancy modules of small aspect ratio. *Appl. Ocean. Res.* **2022**, *120*, 103014. [\[CrossRef\]](#)
- Wu, J.; Lie, H.; Fu, S.; Baarholm, R.; Constantinides, Y. VIV responses of riser with buoyancy elements: Forced motion test and numerical prediction. In Proceedings of the AASME 2017 36th International Conference on Offshore Mechanics and Arctic Engineering, Trondheim, Norway, 25–30 June 2017; Volume 57649. [\[CrossRef\]](#)
- Wu, J.; Lekkala, M.R.; Ong, M.C. Prediction of riser VIV with staggered buoyancy elements. In Proceedings of the ASME 2016 35th International Conference on Offshore Mechanics and Arctic Engineering, Busan, Republic of Korea, 19–24 June 2016; Volume 49934. [\[CrossRef\]](#)
- Wu, J.; Lie, H.; Constantinides, Y.; Baarholm, R.J. NDP riser VIV model test with staggered buoyancy elements. In Proceedings of the ASME 2016 35th International Conference on Ocean, Offshore and Arctic Engineering, Busan, Republic of Korea, 19–24 June 2016. [\[CrossRef\]](#)

21. Lekkala, M.R.; Mohamed, L.; Hafiz, M.F.U.; Kim, D.K. A practical technique for hydrodynamic coefficients modification in SHEAR7 for fatigue assessment of riser buoyancy modules under vortex-induced vibration. *Ocean. Eng.* **2020**, *217*, 107760. [CrossRef]
22. Ma, Y.; Xu, W.; Ai, H.; Wang, Y.; Jia, K. The effect of time-varying axial tension on VIV suppression for a flexible cylinder attached with helical strakes. *Ocean. Eng.* **2021**, *241*, 109981. [CrossRef]
23. Guo, L.; Yuan, Y.; Tang, W.; Xue, H. Experimental investigation on vortex-induced vibration of marine towing cable with suppression device. *Ocean. Eng.* **2023**, *269*, 113531. [CrossRef]
24. Xu, W.; Luan, Y.; Han, Q.; Ji, C.; Cheng, A. The effect of yaw angle on VIV suppression for an inclined flexible cylinder fitted with helical strakes. *Appl. Ocean. Res.* **2017**, *67*, 263–276. [CrossRef]
25. Xu, W.-H.; Qin, W.-Q.; He, M.; Gao, X.-F. Passive VIV reduction of an inclined flexible cylinder by means of helical strakes with round-section. *China Ocean. Eng.* **2018**, *32*, 413–421. [CrossRef]
26. Lauria, A.; Loprieno, P.; Rizzo, F.; Severini, A.; Foti, D.; Leone, E.; Francone, A.; Tomasicchio, G. On the effects of wind and operating conditions on mooring line tensions for floating offshore wind turbine. *Appl. Ocean. Res.* **2024**, *152*, 104197. [CrossRef]
27. Tomasicchio, G.R.; Avossa, A.M.; Riefolo, L.; Ricciardelli, F.; Musci, E.; D'Alessandro, F.; Vicinanza, D. Dynamic Modelling of a Spar Buoy Wind Turbine. In Proceedings of the ASME 2017 36th International Conference on Ocean, Offshore and Arctic Engineering, Trondheim, Norway, 25–30 June 2017. [CrossRef]
28. Cloutier, L.; Diana, G.; Goel, A.; Hardy, C.; Lilien, J.; Wang, J. *EPRI Transmission Line Reference Book: WIND-Induced Conductor Motion*; EPRI: Palo Alto, CA, USA, 2006; pp. 1–400. Available online: <https://hdl.handle.net/11311/255614> (accessed on 15 September 2024).
29. Chan, J.; Havard, D.; Rawlins, C.; Diana, G.; Cloutier, L.; Lilien, J.L.; Hardy, C.; Wang, J.; Goel, A. *EPRI Transmission Line Reference Book: Wind-Induced Conductor Motion*; EPRI: Palo Alto, CA, USA, 2009; p. 1018554. Available online: <https://hdl.handle.net/2268/102166> (accessed on 15 September 2024).
30. Wang, Y.; Liu, Z.; Yang, C.; Brownjohn, J.; Hua, X.; He, J.; Chen, Z. Stagnation point-induced vibration on ultra-long stay cables and the vibration control by using a novel stockbridge damper. *J. Wind. Eng. Ind. Aerodyn.* **2023**, *241*, 105535. [CrossRef]
31. Berthelley, J.; Sievert, D.; Berton, É.; Quentin, P. Stockbridge dampers for extending the fatigue life of a cable at St Nazaire cable stayed bridge. *Eng. Fail. Anal.* **2022**, *141*, 106581. [CrossRef]
32. Nie, X.; Tan, T.; Yan, Z.; Zhang, W. Ultra-wideband piezoelectric energy harvester based on Stockbridge damper and its application in smart grid. *Appl. Energy* **2020**, *267*, 114898. [CrossRef]
33. Sauter, D.; Hagedorn, P. On the hysteresis of wire cables in Stockbridge dampers. *Int. J. Non-Linear Mech.* **2002**, *37*, 1453–1459. [CrossRef]
34. Vaja, N.; Barry, O.; Tanbour, E. On the modeling and analysis of a vibration absorber for overhead powerlines with multiple resonant frequencies. *Eng. Struct.* **2018**, *175*, 711–720. [CrossRef]
35. Kim, S.; Kim, S.; Kim, H.-K. High-mode vortex-induced vibration of stay cables: Monitoring, cause investigation, and mitigation. *J. Sound Vib.* **2022**, *524*, 116758. [CrossRef]
36. Martinelli, L.; Lamberti, A.; Ruol, P.; Ricci, P.; Kirrane, P.; Fenton, C.; Johanning, L. Power umbilical for ocean renewable energy systems-feasibility and dynamic response analysis. In Proceedings of the 3rd International Conference on Ocean Energy, Bilbao, Spain, 6–8 October 2010. Available online: <https://www.researchgate.net/publication/228814942> (accessed on 15 September 2024).
37. Thies, P.R.; Johanning, L.; Smith, G.H. Assessing mechanical loading regimes and fatigue life of marine power cables in marine energy applications. *Proc. Inst. Mech. Eng. Part O J. Risk Reliab.* **2012**, *226*, 18–32. [CrossRef]
38. Rentschler, M.U.; Adam, F.; Chainho, P. Design optimization of dynamic inter-array cable systems for floating offshore wind turbines. *Renew. Sustain. Energy Rev.* **2019**, *111*, 622–635. [CrossRef]
39. Zang, Z.; Chen, Z.; Zhao, M.; Xu, W.; Chen, Y. Experimental study on dynamic responses of a tensioned flexible vertical cylinder under waves and combined current and waves. *Ocean. Eng.* **2022**, *266*, 113159. [CrossRef]
40. Brown, D. Video modeling: Combining dynamic model simulations with traditional video analysis. In Proceedings of the American Association of Physics Teachers (AAPT) Summer Meeting, Edmonton, AB, Canada, 19–23 July 2008. Available online: https://tracker.physlets.org/download/video_modeling.pdf (accessed on 15 September 2024).

Disclaimer/Publisher's Note: The statements, opinions and data contained in all publications are solely those of the individual author(s) and contributor(s) and not of MDPI and/or the editor(s). MDPI and/or the editor(s) disclaim responsibility for any injury to people or property resulting from any ideas, methods, instructions or products referred to in the content.